



University of Zurich

# Wave Length Shifting Reflectors in Liquid Argon for the ArDM Experiment

Bachelor thesis

Mario Thomann

March 2008

## **Abstract**

The driving force for the ArDM experiment is to search for weak interacting massive particles, WIMPs, a popular candidate for cold non-baryonic dark matter.

A one-ton liquid argon (LAr) time projection chamber (TPC) is in development to detect interactions between WIMPs and matter. WIMP - argon interaction produces light and charge by scintillation and ionization. A first version of the light readout system and the reflectors has been assembled at CERN and tested with LAr.

The light readout system has been developed in a small LAr cell. The goal of my thesis is to test different configurations of wavelength shifting reflectors in LAr. With the collected data I determine the number of photoelectrons for each reflector. Additional measurements have been done in gaseous argon.

## Contents

<b>1</b>	<b>Introduction</b>	<b>3</b>
1.1	Dark Matter . . . . .	3
1.2	ArDM Experiment . . . . .	3
<b>2</b>	<b>Experimental Setup</b>	<b>6</b>
2.1	Wavelength Shifter and Reflector Construction . . . . .	6
<b>3</b>	<b>Measurements in Liquid and Gaseous Argon</b>	<b>12</b>
<b>4</b>	<b>Electronics and Data Acquisition</b>	<b>14</b>
<b>5</b>	<b>Data Analysis</b>	<b>14</b>
5.1	Gaseous Argon Series . . . . .	15
5.2	LAr measurement with 1.1 mg/cm <sup>2</sup> TPB surface density . . .	18
5.2.1	Description . . . . .	18
5.2.2	Results . . . . .	18
5.3	LAr measurement with 0.55 mg/cm <sup>2</sup> TPB surface density . .	21
5.3.1	Description . . . . .	21
5.3.2	Results . . . . .	22
5.4	LAr measurement with 0.8 mg/cm <sup>2</sup> TPB surface density. . .	25
5.4.1	Description . . . . .	25
5.4.2	Results . . . . .	25
5.5	LAr measurement with 0.25 mg/cm <sup>2</sup> TPB surface density . .	28
5.5.1	Description . . . . .	28
5.5.2	Results . . . . .	29
5.6	Single Photon Calibration . . . . .	32
5.7	Quartz Plate Series in Gaseous Argon . . . . .	32
<b>6</b>	<b>Summary</b>	<b>33</b>
<b>7</b>	<b>Final Results and Conclusion</b>	<b>33</b>
<b>8</b>	<b>Acknowledgements</b>	<b>36</b>
<b>9</b>	<b>Glossary</b>	<b>37</b>

## List of Tables

1	The table shows the first and third series of the LAr measurement for the reflector with 1.1 mg/cm <sup>2</sup> TPB surface density.	20
2	LAr data for the reflector with 0.55 mg/cm <sup>2</sup> TPB surface density. There are the data of the first, second and third series listed. . . . .	24

---

3	On the table are the first, second and third LAr data series listed for the reflector with $0.8 \text{ mg/cm}^2$ TPB surface density.	27
4	On the table are the LAr data of the first, second and third series listed for the reflector with $0.25 \text{ mg/cm}^2$ TPB surface density . . . . .	31

# 1 Introduction

## 1.1 Dark Matter

On large scales gravity has much bigger influence on the happening in the universe than expected from visible baryonic matter. This is shown by spiral galaxies like the Milky Way for example. The stars on the outer border of our galaxy rotate much faster around the centre than the Newtonian gravity laws applied on visible matter allow it. The same phenomenon is observable on the next higher scale in the universe: the galaxy clusters. Fritz Zwicky<sup>1</sup> already remarked in 1930 that the galaxies rotate so fast that the gravity of the visible matter shouldn't be able to keep the cluster together. The name "dark matter" was invented when he studied the Coma cluster.

This and other observations such as the fluctuation of the cosmic microwave radiation or data from the Hubble telescope<sup>2</sup> drove the physicist to the model of dark matter.

Physicists expect that the universe consists of 23% dark matter, 4% baryonic (visible) matter and an amount of 73% dark energy. The current candidate for dark matter is the lightest so-called super symmetric SUSY particle, the neutralino  $\tilde{\chi}_1^0$ . Because it is the lightest SUSY particle it should not decay.

The standard model of particle physics (SM) is an incomplete approach for two reasons: The weak, strong and electromagnetic force are expected to converge at an energy scale of  $10^{16}$  GeV but they do not converge in the SM. Second: we have to fix free parameters.

In 1974, the first model that was able to solve this problem was constructed by Glashow and Georgi based on SU(5) symmetry. The problem in the SM is the diverging Higgs mass to infinity. In the minimal supersymmetric standard model (MSSM) a spin-1/2-SUSY partner accompanies every spin-0 or spin-1-boson and a spin-0-SUSY partner accompanies every spin-1/2-fermion. This mechanism eliminates the divergence of the Higgs mass. In MSSM exists five Higgsbosons:  $h^0$ ,  $H^0$ ,  $A^0$ ,  $H^+$  and  $H^-$ . The  $h^0$ ,  $H^0$ ,  $A^0$  are mixing with the zino, the  $Z^0$ , and produce the neutralino states  $\tilde{\chi}_1^0$ ,  $\tilde{\chi}_2^0$ ,  $\tilde{\chi}_3^0$ ,  $\tilde{\chi}_4^0$  [1].

## 1.2 ArDM Experiment

A liquid argon detector is in development at CERN<sup>3</sup> to measure in a future experiment interactions between WIMPs and argon.

---

<sup>1</sup>Swiss-American physicist and astronomer, 1898 - 1974

<sup>2</sup>Hubble Space Telescope launched on April 24 1990

<sup>3</sup>The European Organization for Nuclear Research is based in Geneva, Switzerland and was founded in 1952.

The WIMP interaction causes recoiling nuclei that ionize and excite neighbouring argon atoms. Ionization produces electrons that can be read out, while excitation produces photons (see fig. 1). These two production components are important for WIMP identification.

As shown in fig. 1 excited  $Ar_2^*$  molecules are produced. In liquid argon they occur in two different states, a triplet  $^3\Sigma_{+u}$  and a singlet  $^1\Sigma_{+u}$  molecular state. They decay with different time constants in a narrow band around 128 nm. The ratio of light to ionization charge is very high for heavily ionizing particles such as recoil nuclei from WIMPs. This allows WIMP interaction to be distinguished from background. The argon isotope  $^{39}\text{Ar}$  is a  $\beta$ -emitter and contributes also to the background.

The ArDM experimental setup is illustrated in fig. 2. Electrons from ionizing recoils are accelerated upwards by the high E-field (5 kV/cm), that is produced by the Greinacher chain (E-field shaping and HV multiplier, shown on fig. 3). The electrons are extracted to the gas phase and read out by the Large Electron Multiplier (LEM) detector. The scintillation light is emitted isotropically in the vacuum ultra-violet (VUV) range  $(120 \pm 10)\text{nm}$  and converted to blue light. It is measured by cryogenic PMTs (photomultiplier tubes) on the bottom (fig. 4) of the setup. The wavelength shift of the VUV light is important due to the sensitivity peak of the alkali photocathode (fig. 9) in the PMTs. This is achieved by the wavelength shifting substance Tetra Phenyl Butadiene (TPB) on the side wall reflectors (further definition see section 2.1) and on the front plate of the photomultiplier tubes.

The PMTs are designed for cryogenic conditions due to liquid argon ( $T = 85\text{ K}$ ) as detection media.

In figure 2 we see the location of the wavelength shifting (WLS) side reflectors in the ArDM setup. With these reflectors the measured light increases significantly. But there are still open questions about the technical aspects like the surface density of the wavelength shifting substance TPB. In this thesis I focus among other things on this problem

The light yield dependence of TPB surface density has been studied in gaseous argon [2]. In my work I used four reflectors with different TPB surface densities and analyzed the luminescence data under LAr conditions using a small LAr cell.

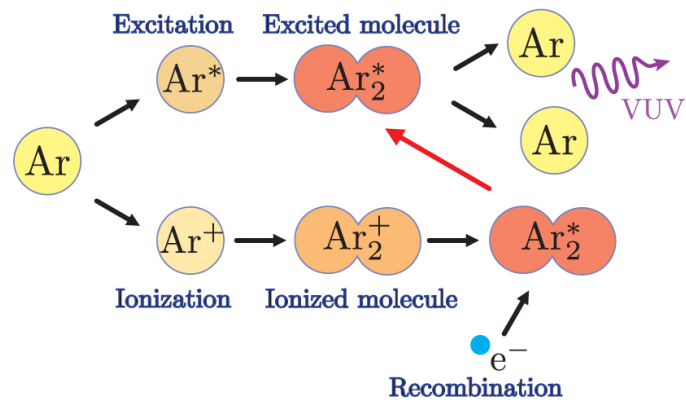


Figure 1: Two light production mechanism in argon (adapted from ref. [3])

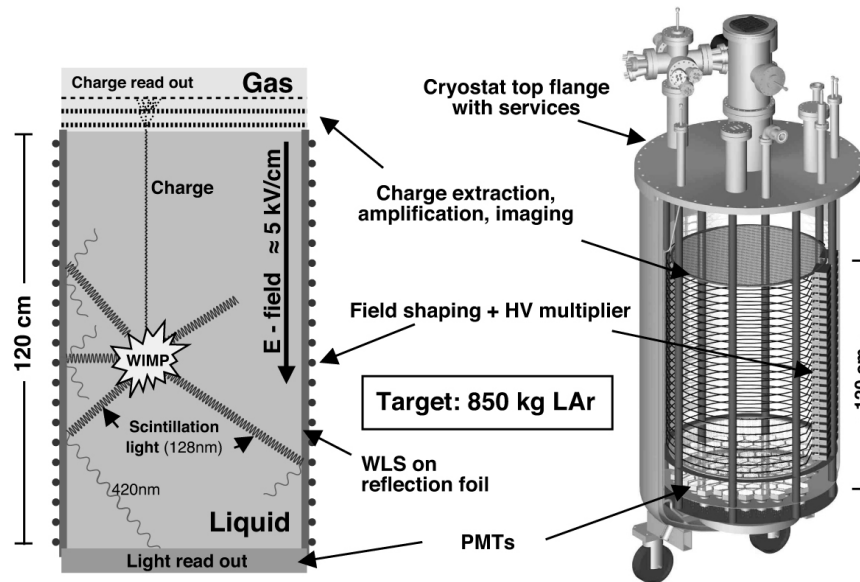


Figure 2: ArDM principle and experimental setup (adapted from ref. [4]).



Figure 3: The photograph shows the high voltage divider of the 1-ton setup during maneuvering with the crane.



Figure 4: On the photograph we see the cryogenic photomultipliers and their support on the bottom of the 1-t setup during assembly.

## 2 Experimental Setup

The stainless steel vessel (fig. 5) with a volume of about 6l encloses two front-to-front mounted Hamamatsu R6237-01mod PMTs (fig. 7) and the whole support. Furthermore the experimental setup consists of four side reflectors (see fig. 6) and a 40 Bq internal  $^{210}\text{Pb}$  source (5.3 MeV  $\alpha$ , 1.2 MeV  $\beta$ ) used for the excitation of argon atoms. Around the PMTs is a Faraday cage installed to eliminate external E-fields.

The vessel has several supply tubes for: signal and high voltage cables of the PMTs; turbo pump / pre-vacuum pump connection; argon cartridge; quadrupole mass spectrometer; security valve; pressure and temperature sensors.

### 2.1 Wavelength Shifter and Reflector Construction

During this thesis I measured the light collection efficiency for different wavelength shifting surface densities on the reflectors in liquid argon. An optimization of the surface density of TPB has been done in gaseous argon by Hugo Cabrera [2].

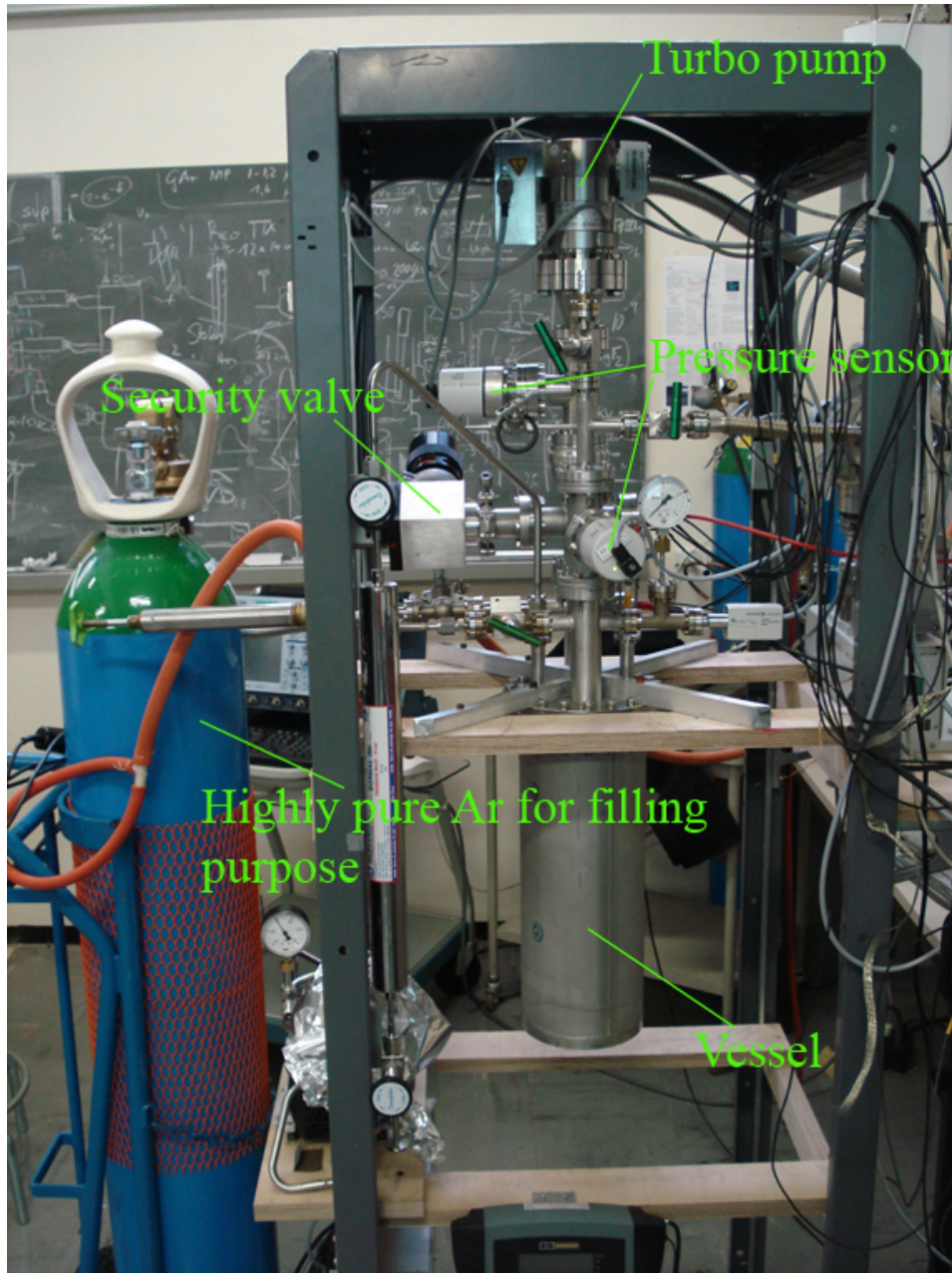


Figure 5: Close view of the prototype light readout setup with the argon cell.



Figure 6: Open setup with mounted reflectors (shiny and reflecting surface with white borders)

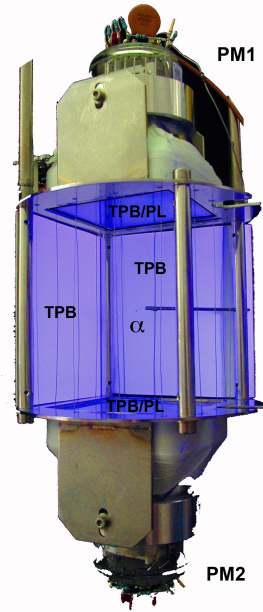


Figure 7: The two facing PMTs in the experimental setup, diameter 14 cm , height about 30 cm

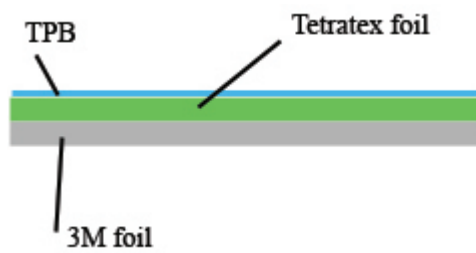


Figure 8: Reflector layout

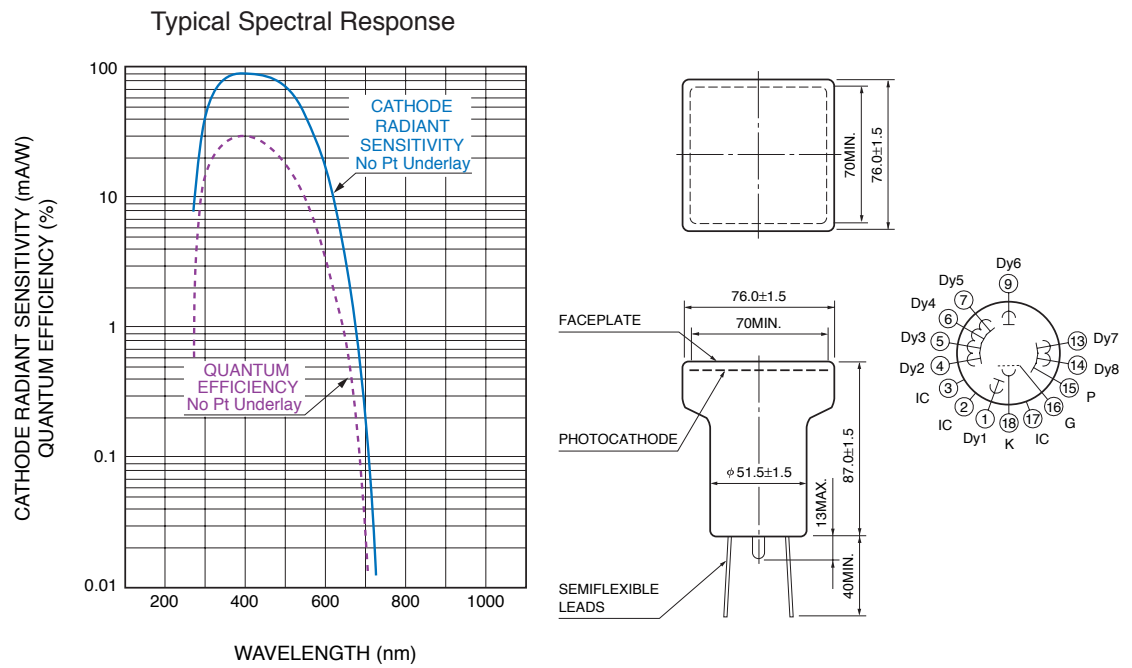


Figure 9: Technical Data of the Hamamatsu R6237-01mod photomultiplier



Figure 10: Cryogenic photomultiplier Hamamatsu R6237-01mod experimental for low temperature, dimensions see in fig 9

As we see in fig. 8 we used for the side reflector three components:

- On top of the reflector is the wavelength shifting substance Tetra Phenyl Butadiene (TPB) evaporated,
- The Tetratex (TTX) membrane (White Tetratex PTFE membrane), which provides permeability to gases, chemical inertness, diffusion of UV-photons and softness at cryogenic temperature is used as a basis for the TPB,
- A metal free multilayer polymeric film is used as Tetratex support. It is produced by 3M Vikuiti and categorized as an Enhanced Specular Reflector (ESR) foil. Vikuiti ESR is highly reflective (98.5%) over the entire visible spectrum and absorbs wavelengths below 350 nm [5],

The Tetratex is welded on the 3M foil that features also non-conductive property (fig. 13). With this characteristic it is possible to place the reflector in the very strong electrical drift field of the one-ton setup. In the light readout setup we installed the reflectors on each of the four side walls (fig. 6 / 14).

The evaporation process of the TPB was made in the group owned large-scale evaporator (fig. 11). We are able to evaporate a surface of 120 x 30 cm<sup>2</sup>.

The surface concentration of TPB on the Tetratex foil is proportional to the load of the crucibles (fig. 12). Above the crucible the Tetratex foil is tightened on wires in an arch shaped assembly. The evaporator is placed in a vacuum chamber. To run the evaporation we decrease the pressure to about 10<sup>-6</sup> mbar and heat the crucibles with a current of 2A and a voltage of 10V. The evaporation process is slow and takes about 3 hours.

The starting position for my measurements is a reflector of (1.10±0.03)mg/cm<sup>2</sup> TPB surface density that is already installed in the setup. Additionally I evaporated three different reflector series with (0.25±0.03) mg/cm<sup>2</sup>, (0.55±0.03) mg/cm<sup>2</sup> and (0.8±0.03) mg/cm<sup>2</sup> [which corresponds to (0.10±0.01) g/crucible, (0.20±0.01) g/crucible and (0.30±0.01) g/crucible].

The front plates of the PMTs are also coated with TPB. We dissolved the TPB in Chloroform together with a plastic matrix (Polystyrene). We filled the liquid mixture in a container and dipped the well-cleaned front plate of the PMT in the liquid. The crucial point of this procedure is to get a homogeneous coverage on the PMT.

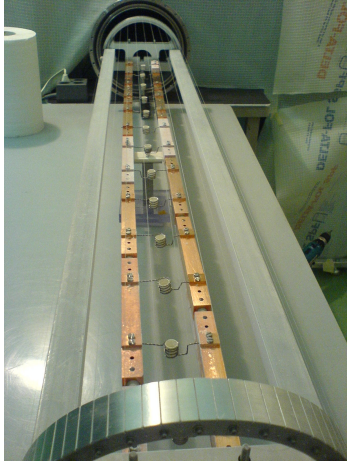


Figure 11: Open large scale evaporator

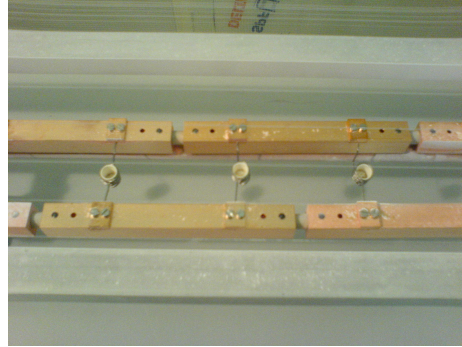


Figure 12: Section of the evaporator and the crucible (white cups)

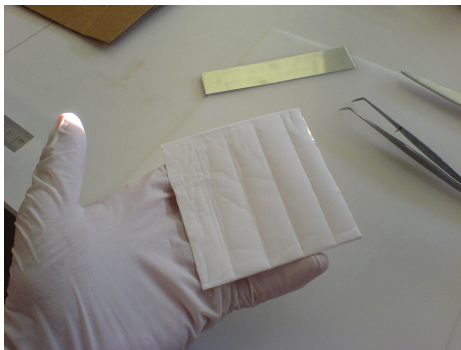


Figure 13: Finished reflector with evaporated TPB on the surface of the white Tetratex foil.



Figure 14: Detached PMT with support during installation of the reflectors.

### 3 Measurements in Liquid and Gaseous Argon

The described setup is suitable for gas and liquid measurements. The scintillation light properties (yield of the scintillation and decay times of the two components) are very sensitive to gas/liquid purity conditions [6].

There are different types of impurities. One kind of impurity absorbs the scintillation light of the 128 nm band and reemits the light in a non-measured wavelength. This leads to a reduction of measured light. Other impurities are strongly polarized molecules that decrease the decay time of the excited argon molecules. In order to avoid contamination with impurities such as water, oxygen and CO<sub>2</sub> all metallic part were cleaned with acetone and plastic parts with ethylene alcohol. The vessel was closed with a copper seal and pumped down to  $10^{-6} \div 2 \cdot 10^{-7}$  mbar in 2  $\div$  4 days. A thermogun was used to warm up softly the vessel to help evaporation of residual water on the internal surface since baking was not possible. The measurements were done with class 60 Ar "detection media"<sup>4</sup> which has the highest quality available commercially. Bulk liquid argon and bulk liquid nitrogen was used as coolants.

The liquefaction procedure was a very delicate step. To speed up the process I filled the outside dewar with a mixture of LN<sub>2</sub> (boiling point 77 K) and LAr in order to reach a temperature between the solidification point and the boiling point of Argon (respectively 85 K and 88 K at 1 atm).

Then gas was let in the setup at a flow of roughly 2 l/min, keeping an inner pressure of about 900mbar. The liquefaction process usually took 2h - 3h, as one can see from fig. 15 in which I report the time evolution of the temperature for different sensors in the setup.

When a temperature sensor touches liquid argon one can observe a knee in the temperature curve of this sensor. A floater mounted on top of the vessel sends a signal as soon as the LAr reaches the top of the vessel.

For fast liquefaction it is important to keep the dewar full. After the first stage of liquefaction the external dewar was filled only with LAr. LN<sub>2</sub> is in fact evaporating much faster than LAr, leaving after 1/2 h almost only LAr in the cooling bath. The level of argon in the external cooling bath has been kept high in order to keep the clean liquid in the inner dewar in thermal equilibrium (and to avoid unwanted pressure increase). During the measurement we kept the setup absolutely tight and the security valve locked. For safety reasons we have to monitor the whole process to prevent any dangerous situation due of quick increasing pressure.

In liquid argon we expect more photons than in gaseous argon. The 5.3 MeV  $\alpha$ -particles produce in liquid at maximum purity  $\sim 210$  K photons [7] and in gaseous argon  $\sim 78$  K [9] photons at 1 bar.

<sup>4</sup>impurity  $\leq 0.5$  ppm H<sub>2</sub>O,  $\leq 0.1$  ppm O<sub>2</sub>,  $\leq 0.5$  ppm N<sub>2</sub> - Data by ALPHAGAS

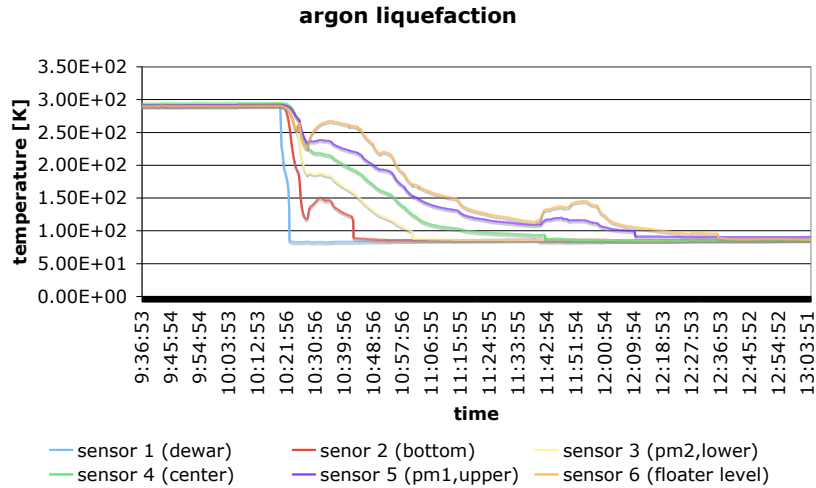


Figure 15: Temperature chart of the Nov 14 2007 liquefaction process for different sensors

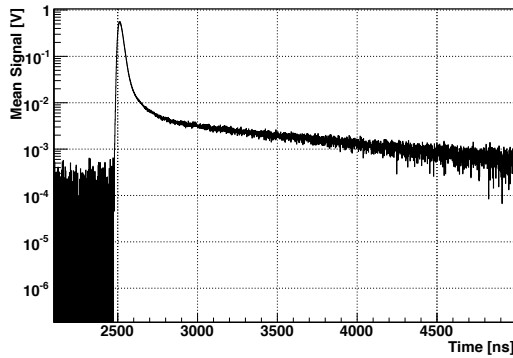


Figure 16: Typical average pulse shape in LAr. It is the mean light signal over the first 5000 events of the upper photomultiplier (Ch1). The decay time of the slow decay component is approximately  $1 \mu\text{s}$ , for correct interpretation pay attention to log y scale

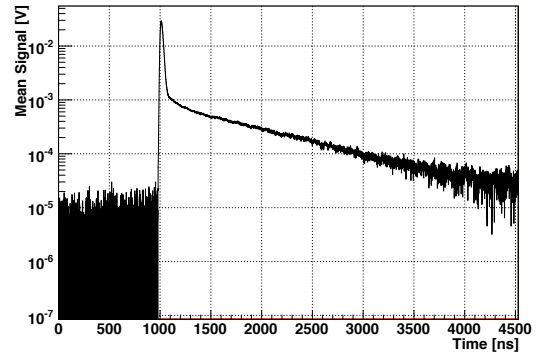


Figure 17: Typical average pulse shape in gaseous argon. It is the mean light signal over the first 2000 events of the upper photomultiplier (Ch1). The decay time of the slow decay component is approximately  $3 \mu\text{s}$ , for correct interpretation pay attention to y scale

## 4 Electronics and Data Acquisition

The two Hamamatsu R6237-01mod PMTs are powered at a standard voltage of 1400 V by a 2 channel programmable HV power supply. A 1 GS/s (20 GS/s were possible) LeCroy oscilloscope with 8-bit resolution acquired the data of the signal of both PMTs. The upper PMT was labeled as Ch1 and the lower PMT as Ch2.

The data was stored on the internal hard-disk of the oscilloscope in compact MatLab format. One measurement series consists of about 10 files with 2'000 to 5'000 events each file. An event is composed of 2 sampled waveforms (5'000 to 10'000 samples) corresponding to the signal that is generated by the two PMTs (detailed values are in the measurement descriptions).

To record an event we used the trigger function of the oscilloscope. A logical "OR" trigger and a threshold trigger setting was used. If the signals reach a certain level (in the range of -20 mV to -100 mV) on one of the two channels, the oscilloscope started to measure both channels (detailed trigger settings and values are in the measurement descriptions).

For measurements in gaseous argon and for the single photon calibration a fast NIM amplifier was needed due to the lower signal amplitude compared to LAr measurements.

## 5 Data Analysis

After data files have been collected I proceed with the off-line analysis by using ROOT (object oriented framework for data analysis based on C++).

For each event we calculate:

- The background (pedestal) averaging 500 samples of the waveform before the trigger and subtracted to the following sample,
- The pulse height (PH) or peak value by looking for the maximum voltage in the acquired time window,
- The peak value time,
- The integrated pulse height (IPH) that is the integral of the signal obtained by summing up the value of all the samples from the "trigger" to the end which correspond to the charge that is generated by the photomultiplier [Charge= IPH (nVs)/50  $\Omega$ ],
- The average pulse shape, that is the light signal averaging over the number of events (fig. 16),

- The component ratio (CR) that is the integral of the first 50ns (IPH50) divided by the total integral (IPH),

To have a quick look on the measured data we used several one- and two-dimensional histograms like fig. 16 or 17. Those give us the possibility to look at the distribution of several thousand events and to pursue a fast plausibility check of the collected data.

In fig. 18 for example we see the correlation between the pulse height and the component ratio variable. With that kind of plot it is possible to identify different particles as shown in fig. 19. Since we are interested in  $\alpha$ -particles we reject data from the  $\mu$ -band as well as the low energy electrons and isolate the  $\alpha$ -particles. The  $\mu$ -band is caused by cosmic  $\mu$  and the low energy electrons by the decay of  $\text{Bi210} \rightarrow \text{Po210}$  in the internal source. The  $\alpha$ -particle event selection is done by choosing an appropriate range of the pulse height (PH) and the integrated pulse height (IPH).

We can also derive some other important quantities from these histograms. We calculate for example the average pulse shape, which is used to study the time dependence of the signal. From fig. 20 for example (semi log scale) we can clearly see two different exponential decays corresponding to the slow  $\tau_2$  and fast  $\tau_1$  component.  $\tau_2$  can be obtained by fitting ( $\chi^2$ -method) the tail of the average pulse shape distribution with an exponential fit.

From previous experiments it is known that the decay time of the slow component  $\tau_2$  is strongly correlated with the gas/liquid purity [3] and decreases with time, while the fast component  $\tau_1$  remains constant for reasonable purity conditions. But because of the higher density in liquid the decrease of  $\tau_2$  presumably due to outgassing takes a longer time than in gaseous argon.

### 5.1 Gaseous Argon Series

As in the previous section described, depends the decay time on the slow component  $\tau_2$  on purity and decrease with time. The fast scintillation component does not show a significant purity dependance in decay time.

The decrease of  $\tau_2$  is clearly observable in figure 21. The measurement of this series were done with gaseous argon at a pressure of 1100 mbar and a partial air pressure of  $10^{-4}$  mbar. Four files of data sets were acquired with 2000 events and 10'000 samples each. Between the initial time of the measurements of two data sets is a time gap of  $\Delta t = 2$  min. The data from the first file is the black curve, than the blue, red and at last the green curve. The steepness of the curve's tail increases as later the starting point of the acquirement gets. That is equivalent to a decreasing decay time of the slow component  $\tau_2$ .

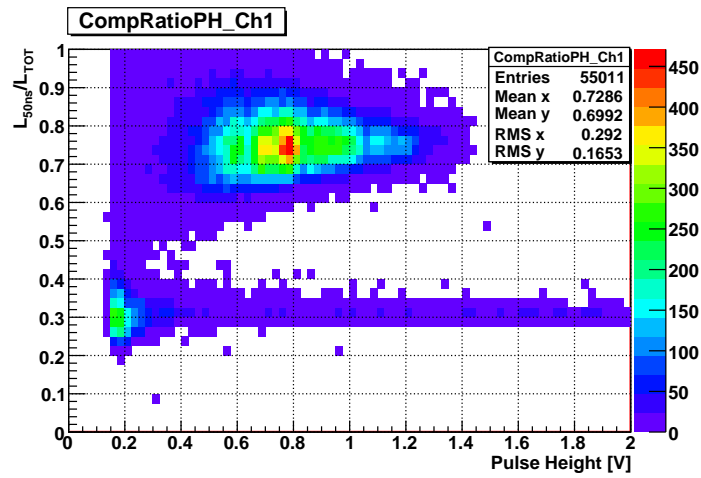


Figure 18: Measurement in LAr for the reflector with  $(1.10 \pm 0.03) \text{mg/cm}^2$  TPB surface density. On the y-axis is the component ratio (see beginning of section 5) and the x-axis shows the peak value of the signal for each event. The colours represent the number of events refer to the scale on the right. The data are from the first series and are acquired from the upper PMT (Ch1).

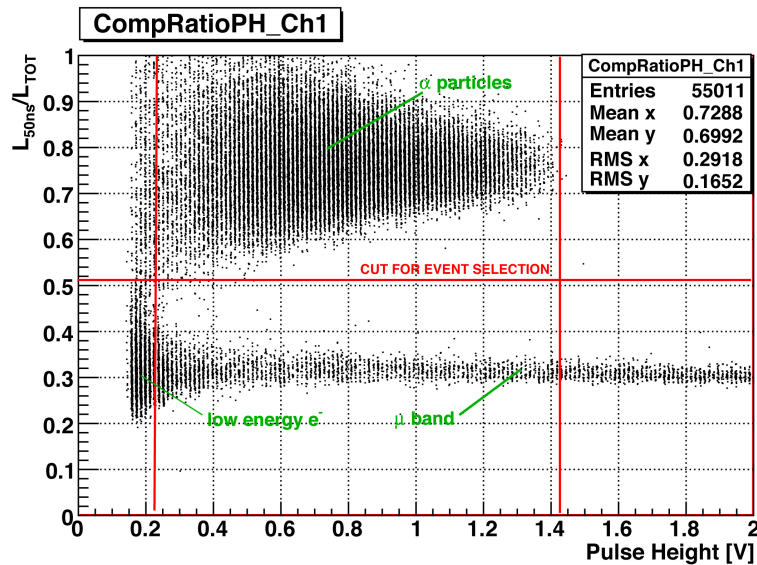


Figure 19: Marked cuts for event selection on the component ratio and on the pulse height for the reflector with  $(1.10 \pm 0.03) \text{mg/cm}^2$  TPB surface density. The upper PMT (Ch1) were used as signal source. The data are from the first series of the liquefied argon. As written in the plot we see events from  $\alpha$ -particles, low energy electrons ( $Q = 1.17 \text{ MeV}$ ) and cosmic muons.

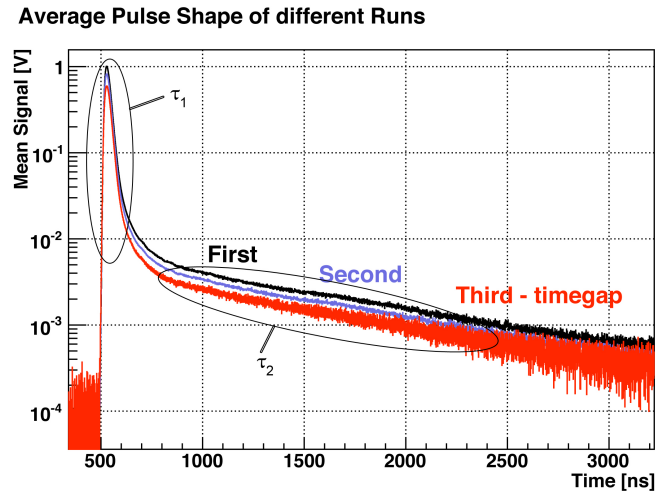


Figure 20: Average pulse shape of a LAr measurement. The three different runs (black, blue and red) distinguish in time of the measurement's start point. The two decay component (fast  $\tau_1$  and slow  $\tau_2$ ) are marked with ellipses.

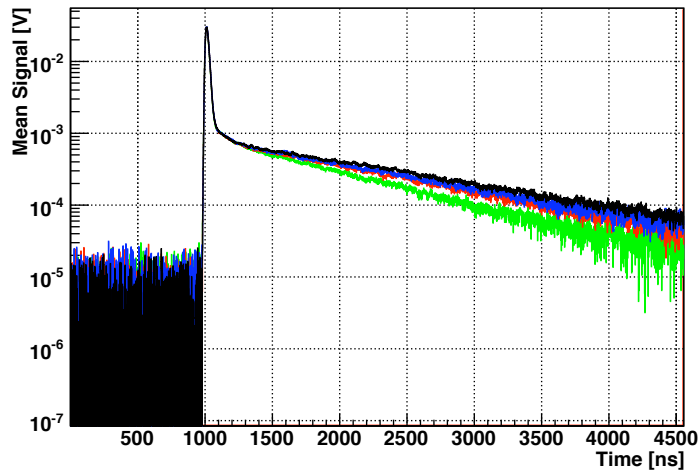


Figure 21: The plot shows the average pulse shape in gaseous argon at a pressure of 1100 mbar and a partial air pressure of  $10^{-4}$  mbar. The time gap between each data set (different colour) is  $\Delta t = 2$  min. The sets are in the order of: black = 1<sup>st</sup>, blue 2<sup>nd</sup>, red = 3<sup>rd</sup> and green = 4<sup>th</sup>. Only events with a pulse height in the range of  $\Delta V = 0.09 - 0.2$  V are considered. Due to increasing impurities (outgassing etc.) we see a change of the signal's tail with increasing time.

## 5.2 LAr measurement with $1.1 \text{ mg/cm}^2$ TPB surface density

### 5.2.1 Description

The reflector with  $(1.10 \pm 0.03) \text{ mg/cm}^2$  TPB surface density was attached on the support. The setup was pumped for 3 days down to  $P_{vessel} = 9 \cdot 10^{-7}$  mbar ( $P_{residual} \approx 10^{-5}$  mbar). After the argon liquefaction process was complete I turned the PMT on and waited  $(20 \div 30)$  min. to let the temperature of the PMT stabilize since the voltage divider is generating heat during operation.

I acquired three data series with the following settings:

- First series: 11 files x 5000 events; gain 300 mV/div; trigger setting  $V_{tr} = -98 \text{ mV Ch1 OR Ch2}$ ;  $P_{vessel} = 820 \text{ mbar}$ ;
- Second series: 11 files x 5000 events; gain 50 mV/div; trigger setting  $V_{tr} = -22 \text{ mV Ch1 OR Ch2}$ ;  $P_{vessel} = 820 \text{ mbar}$ ;
- Third series: 11 files x 5000 events; gain 300mV/div; trigger setting  $V_{tr} = -98 \text{ mV Ch1 OR Ch2}$ ;  $P_{vessel} = 820 \text{ mbar}$ ; timegap between each run of about 10 min.

### 5.2.2 Results

To analyze the data I only used the first and third series. The second series was only used to focus on the low energy part. In fig. 22 we see a typical average pulse shape of the signal over 5000 events and in fig. 23 the IPH over all events of the third series.

In fig. 24 we see that the IPH shifts strongly in the first series compared to the third series where it remains quite more. The  $\tau_2$  changes only marginally.

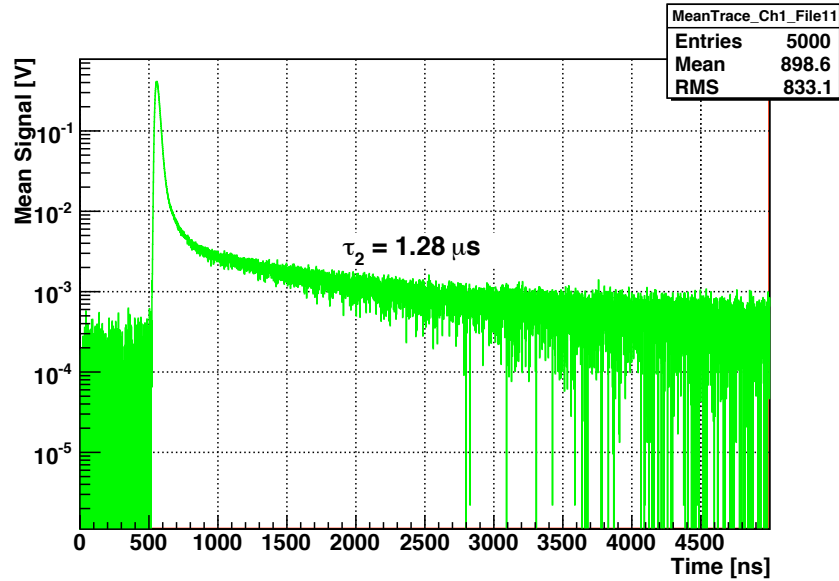


Figure 22: The plot shows the mean signal vs. time of the upper PMT for the reflector with  $1.1 \text{ mg/cm}^2$  TPB surface density. It is the last file of the the third series with the used LAr. The slow decay component  $\tau_2$  has a value of  $1.28 \mu\text{s}$  (fit procedure in the time range of 900 - 2500 ns )

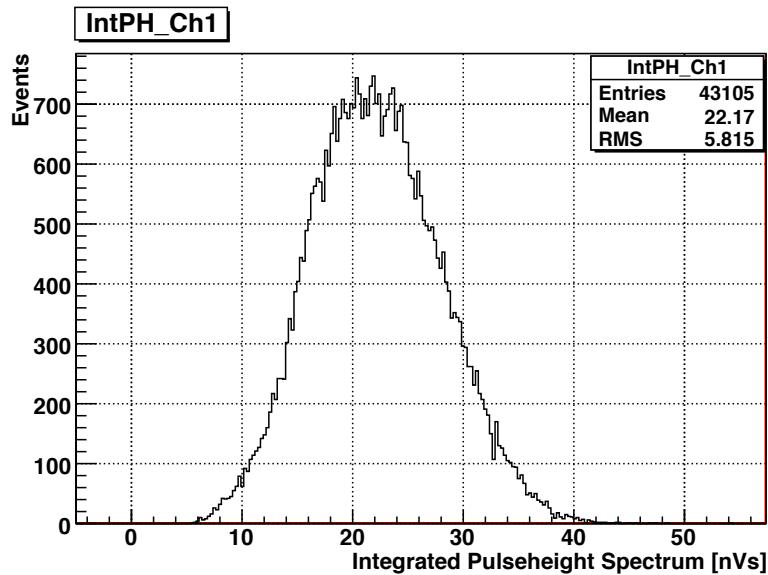


Figure 23: The plot shows the integrated pulse height in LAr for the reflector with  $1.1 \text{ mg/cm}^2$  TPB surface density. The signal source is the upper PMT. We look at the data of all 11 files of the third series.

Table 1: The table shows the first and third series of the LAr measurement for the reflector with  $1.1 \text{ mg/cm}^2$  TPB surface density.

<i>Mean IPH</i> [ <i>nVs</i> ]	$\tau_2$ [ $\mu\text{s}$ ]
$44.02 \pm 0.16$	$1.1 \pm 0.06$
$42.59 \pm 0.15$	$1.2 \pm 0.06$
$40.97 \pm 0.14$	$1.1 \pm 0.06$
$39.48 \pm 0.14$	$1.2 \pm 0.06$
$38.21 \pm 0.13$	$1.2 \pm 0.06$
$36.67 \pm 0.12$	$1.2 \pm 0.06$
$34.86 \pm 0.12$	$1.1 \pm 0.06$
$33.57 \pm 0.12$	$1.1 \pm 0.06$
$32.36 \pm 0.11$	$1.1 \pm 0.06$
$31.45 \pm 0.11$	$1.2 \pm 0.06$
$30.39 \pm 0.10$	$1.1 \pm 0.06$
$22.93 \pm 0.09$	$1.2 \pm 0.06$
$22.86 \pm 0.08$	$1.2 \pm 0.06$
$22.58 \pm 0.08$	$1.2 \pm 0.06$
$22.25 \pm 0.08$	$1.2 \pm 0.06$
$22.07 \pm 0.08$	$1.2 \pm 0.06$
$22.00 \pm 0.08$	$1.1 \pm 0.06$
$21.97 \pm 0.08$	$1.2 \pm 0.06$
$21,95 \pm 0.08$	$1.4 \pm 0.06$
$21.94 \pm 0.08$	$1.2 \pm 0.06$
$21.75 \pm 0.08$	$1.3 \pm 0.06$
$21,68 \pm 0.08$	$1.3 \pm 0.06$

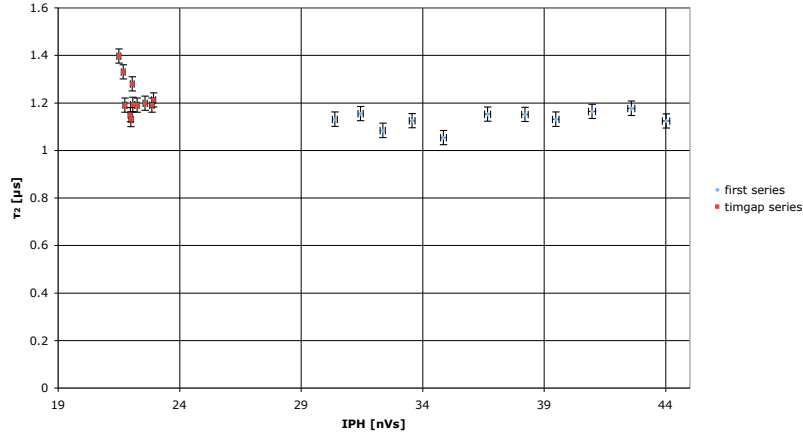


Figure 24: Integrated pulse height vs. short decay component  $\tau_2$  for the reflector with  $1.1 \text{ mg/cm}^2$  TPB surface density of the first and third series.

### 5.3 LAr measurement with $0.55 \text{ mg/cm}^2$ TPB surface density

#### 5.3.1 Description

The reflector with  $(0.55 \pm 0.03) \text{ mg/cm}^2$  TPB surface density was placed on the support. The setup was pumped for 4 days down to  $P_{\text{vessel}} = 9 \cdot 10^{-7} \text{ mbar}$  ( $P_{\text{residual}} \approx 10^{-5} \text{ mbar}$ ). After the liquefaction process of the highly pure argon was complete, the three data series were acquired with the following settings:

- First series: 11 files x 5000 events; gain 300 mV/div; trigger setting  $V_{tr} = -98 \text{ mV Ch1 OR Ch2}$ ;  $P_{\text{vessel}} = 850 \text{ mbar}$ ;
- Second series: 11 files x 5000 events; gain 300 mV/div; trigger setting  $V_{tr} = -98 \text{ mV Ch1 OR Ch2}$ ;  $P_{\text{vessel}} = 850 \text{ mbar}$ ;
- Third series: 6 files x 5000 events; gain 300 mV/div; trigger setting  $V_{tr} = -98 \text{ mV Ch1 OR Ch2}$ ;  $P_{\text{vessel}} = 850 \text{ mbar}$ ; timegap between each run of about 15 min.

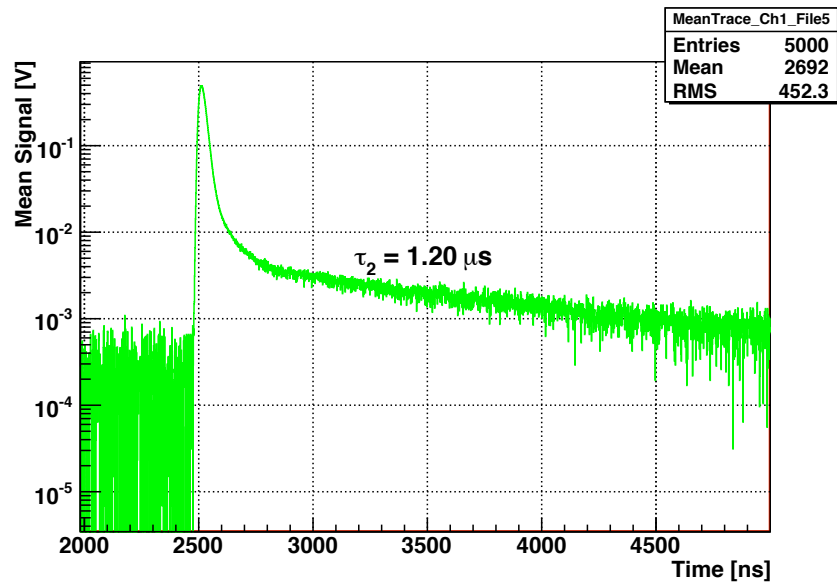


Figure 25: On the plot we see the average pulse shape for the reflector with  $0.55 \text{ mg/cm}^2$  TPB surface density of the last file, third series. The slow decay component  $\tau_2$  has a value of  $1.20 \mu\text{s}$  (fit procedure in the time range of 2900 - 3500 ns )

### 5.3.2 Results

This measurement shows reasonable data and no series had to be rejected. We see in fig. 27 that the IPH shifts a little and the  $\tau_2$  stays stable.

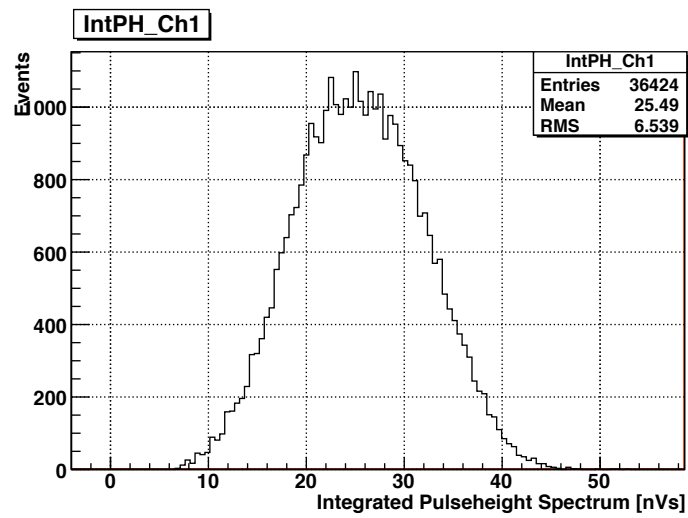


Figure 26: The plot shows the integrated pulse height spectrum for the reflector with  $0.55 \text{ mg/cm}^2$  TPB surface density of the first series.

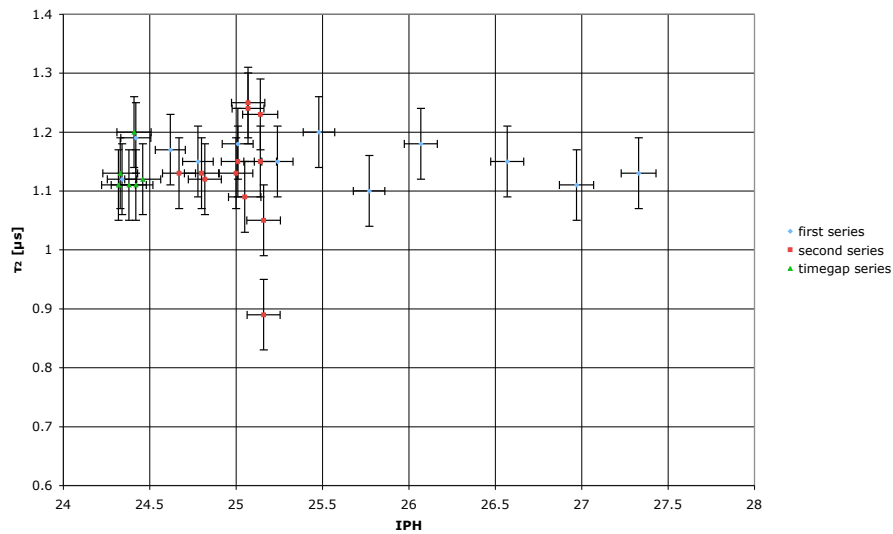


Figure 27: On the plot we see the integrated pulse height vs. the slow decay component  $\tau_2$  for the reflector with  $0.55 \text{ mg/cm}^2$  TPB surface density of the first, second and third series.



## 5.4 LAr measurement with $0.8 \text{ mg/cm}^2$ TPB surface density.

### 5.4.1 Description

The reflector with  $(0.8 \pm 0.03) \text{ mg/cm}^2$  TPB surface density has been installed on the support of the PMTs. The setup was pumped for 3 days down to  $P_{vessel} = 9 \cdot 10^{-7} \text{ mbar}$  ( $P_{residual} \approx 10^{-5} \text{ mbar}$ ). After the argon liquefaction process was finished, I acquired three data series with the following settings:

- First series: 11 files x 5000 events; gain 200 mV/div; trigger setting  $V_{tr} = -98 \text{ mV Ch1 OR Ch2}$ ;  $P_{vessel} = 770 \text{ mbar}$ ;
- Second series: 11 files x 5000 events; gain 200 mV/div; trigger setting  $V_{tr} = -98 \text{ mV Ch1 OR Ch2}$ ;  $P_{vessel} = 880 \text{ mbar}$ ;
- Third series: 4 files x 5000 events; gain 200 mV/div; trigger setting  $V_{tr} = -98 \text{ mV Ch1 OR Ch2}$ ;  $P_{vessel} = 920 \text{ mbar}$ ; timegap between each run of about 20 min.

### 5.4.2 Results

In this LAr measurement the slow decay component  $\tau_2$  is due to an unknown reason very short (around  $0.8 \mu\text{s}$ ). Because of this fact we can't compare these three series with the other measurements directly. We have to make a correction to interpolate the data. In the table 3 we see the analyzed data without the correction factor. In those three series we had a strongly changing pressure (770 mbar - 920 mbar) that may caused also some irregularities in the data. The IPH stays quite stable as we see in fig. 30.

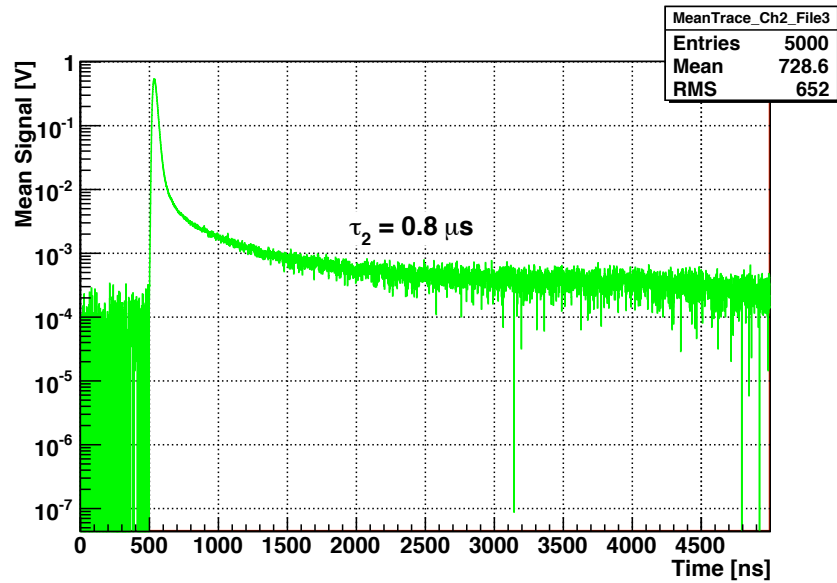


Figure 28: The plot shows the average pulse shape for the reflector with  $0.8 \text{ mg/cm}^2$  TPB surface density. It is the last file, third data series after liquefaction and measured with the upper PMT. The slow decay component  $\tau_2$  has a value of  $0.80 \mu\text{s}$  (fit procedure in the time range of 900 - 2500 ns )

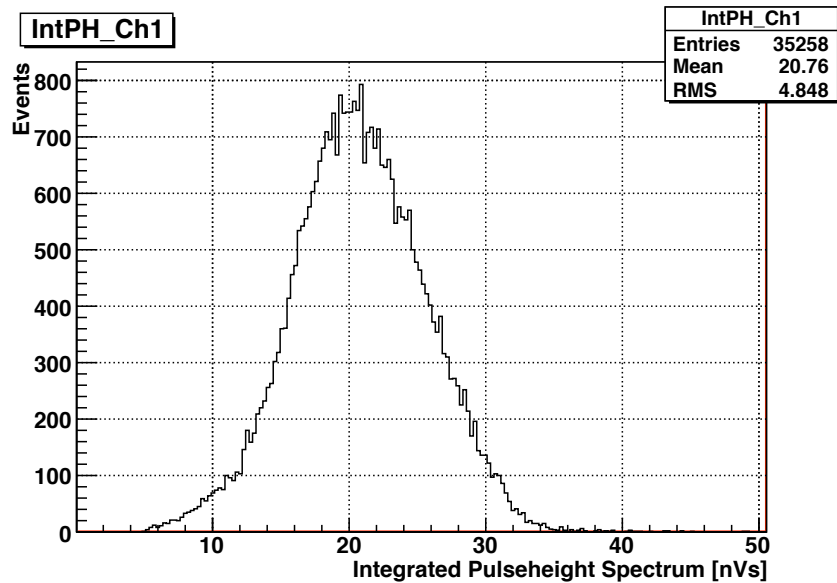


Figure 29: The histogram shows the integrated pulse height spectrum for the reflector with  $0.8 \text{ mg/cm}^2$  TPB surface density of the first series.

Table 3: On the table are the first, second and third LAr data series listed for the reflector with  $0.8 \text{ mg/cm}^2$  TPB surface density.

<i>Mean IPH</i> [ <i>nVs</i> ]	$\tau_2$ [ $\mu s$ ]
$21.09 \pm 0.07$	$0.9 \pm 0.1$
$20.97 \pm 0.07$	$0.8 \pm 0.1$
$21.03 \pm 0.07$	$0.7 \pm 0.1$
$20.69 \pm 0.07$	$0.8 \pm 0.1$
$20.76 \pm 0.07$	$0.8 \pm 0.1$
$20.76 \pm 0.07$	$0.9 \pm 0.1$
$20.56 \pm 0.07$	$0.9 \pm 0.1$
$20.79 \pm 0.07$	$0.8 \pm 0.1$
$20.53 \pm 0.07$	$0.8 \pm 0.1$
$20.51 \pm 0.07$	$0.9 \pm 0.1$
$20.74 \pm 0.07$	$0.7 \pm 0.1$
$20.18 \pm 0.07$	$1.0 \pm 0.1$
$20.04 \pm 0.07$	$0.8 \pm 0.1$
$19.96 \pm 0.06$	$0.7 \pm 0.1$
$19.80 \pm 0.06$	$0.7 \pm 0.1$
$19.74 \pm 0.06$	$0.9 \pm 0.1$
$19.73 \pm 0.06$	$0.8 \pm 0.1$
$19.55 \pm 0.06$	$0.6 \pm 0.1$
$19.54 \pm 0.06$	$0.7 \pm 0.1$
$19.54 \pm 0.06$	$0.9 \pm 0.1$
$19.50 \pm 0.06$	$0.8 \pm 0.1$
$19.06 \pm 0.06$	$0.7 \pm 0.1$
$18.92 \pm 0.06$	$0.7 \pm 0.1$
$18.47 \pm 0.06$	$0.9 \pm 0.1$
$18.45 \pm 0.06$	$0.8 \pm 0.1$

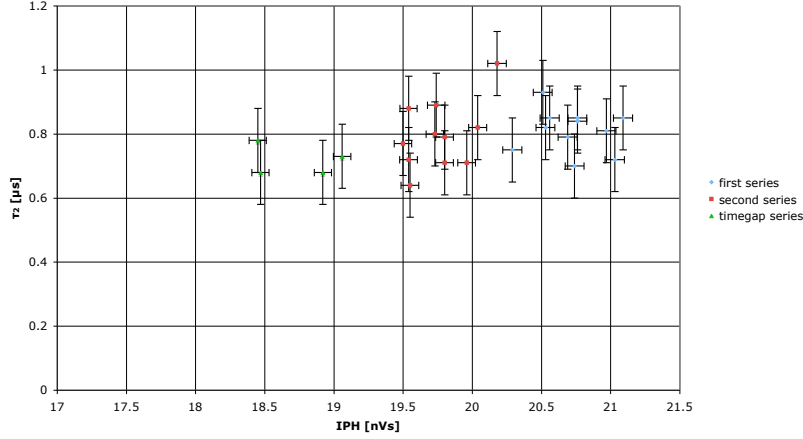


Figure 30: The plot shows the IPH vs.  $\tau_2$  for the reflector with  $0.8 \text{ mg/cm}^2$  TPB surface density of the first, second and third series.

## 5.5 LAr measurement with $0.25 \text{ mg/cm}^2$ TPB surface density

### 5.5.1 Description

The reflector with  $(0.25 \pm 0.03) \text{ mg/cm}^2$  TPB surface density has been installed on the PMT support. The setup was pumped for 3 days down to  $P_{vessel} = 9 \cdot 10^{-7} \text{ mbar}$  ( $P_{residual} \approx 10^{-5} \text{ mbar}$ ). After the argon liquefaction process was complete I turned the PMT on and waited  $(20 \div 30) \text{ min.}$  to let the temperature of the PMT stabilize due to the heat production of the voltage divider during operation.

The following settings was applied for the acquisition of the three data series:

- First series: 11 files x 5000 events; gain 200 mV/div; trigger setting  $V_{tr} = -100 \text{ mV Ch1 OR Ch2}$ ;  $P_{vessel} = 680 \text{ mbar}$ ;
- Second series: 11 files x 5000 events; gain 200 mV/div; trigger setting  $V_{tr} = -100 \text{ mV Ch1 OR Ch2}$ ;  $P_{vessel} = 800 \text{ mbar}$ ;
- Third series: 6 files x 5000 events; gain 200 mV/div; trigger setting  $V_{tr} = -100 \text{ mV Ch1 OR Ch2}$ ;  $P_{vessel} = 860 \text{ mbar}$ ; timegap between each run of about 20 min.

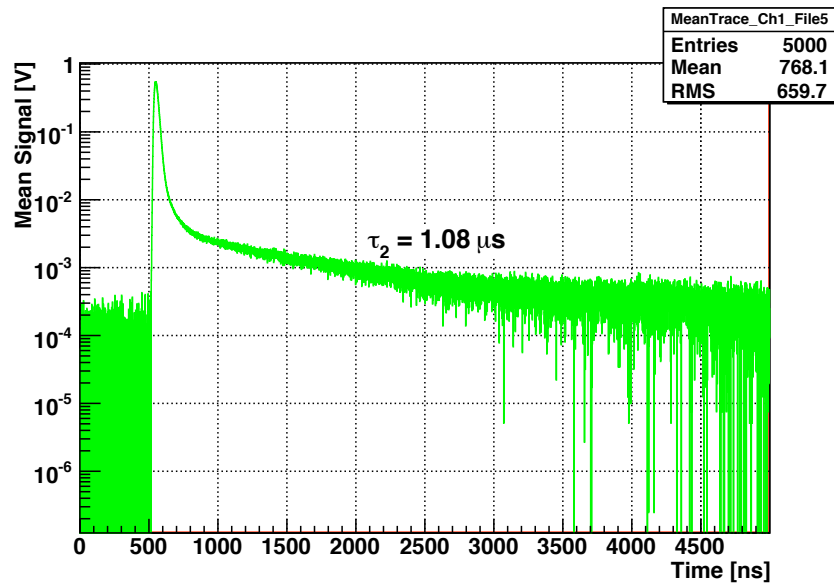


Figure 31: The plot shows the average pulse shape of the last file, third series in LAr for the reflector with  $0.25 \text{ mg/cm}^2$  TPB surface density. The slow decay component  $\tau_2$  has a value of  $1.08 \mu\text{s}$  (fit procedure in the time range of 900 - 2500 ns )

### 5.5.2 Results

The slow decay component  $\tau_2$  stays quite stable while the integrated pulse height changes dramatically as we see in fig. 33.

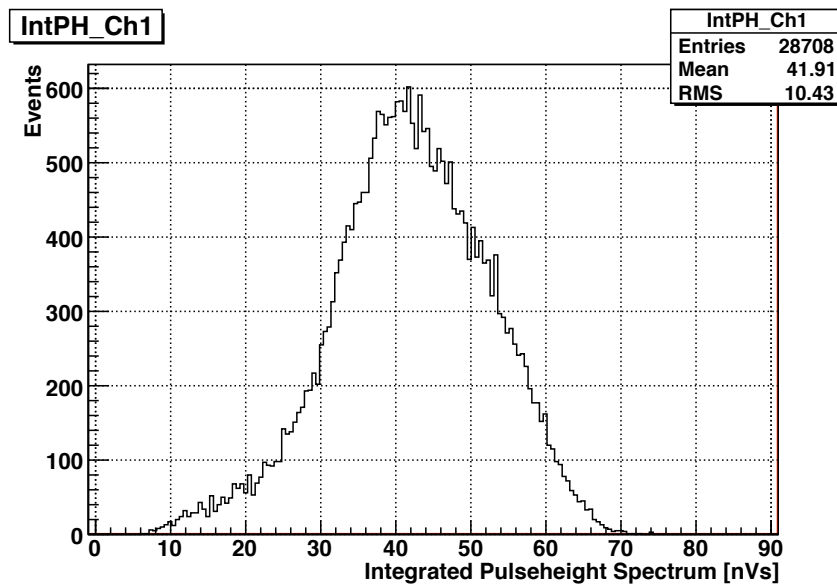


Figure 32: The histogram shows the integrated pulse height spectrum for the reflector with  $0.25 \text{ mg/cm}^2$  TPB surface density from the first series.

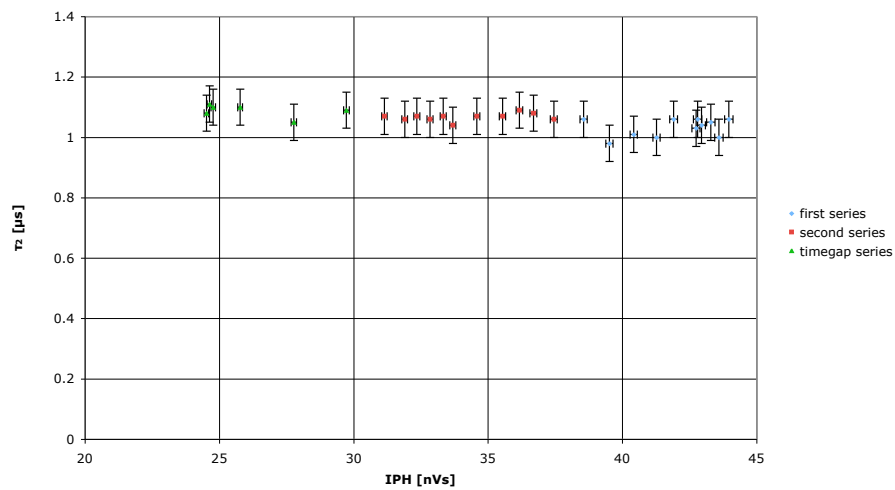


Figure 33: The plot shows the integrated pulse height vs.  $\tau_2$  for the reflector with  $0.25 \text{ mg/cm}^2$  TPB surface density. A strong IPH shift is observable.

Table 4: On the table are the LAr data of the first, second and third series listed for the reflector with  $0.25 \text{ mg/cm}^2$  TPB surface density

<i>Mean IPH</i> [nVs]	$\tau_2$ [ $\mu\text{s}$ ]
$43.59 \pm 0.16$	$1.0 \pm 0.06$
$43.29 \pm 0.16$	$1.1 \pm 0.06$
$43.96 \pm 0.15$	$1.1 \pm 0.06$
$42.74 \pm 0.15$	$1.0 \pm 0.06$
$42.80 \pm 0.15$	$1.1 \pm 0.06$
$42.94 \pm 0.15$	$1.0 \pm 0.06$
$41.91 \pm 0.15$	$1.1 \pm 0.06$
$41.27 \pm 0.14$	$1.0 \pm 0.06$
$40.42 \pm 0.14$	$1.0 \pm 0.06$
$39.52 \pm 0.14$	$1.0 \pm 0.06$
$38.56 \pm 0.13$	$1.1 \pm 0.06$
$37.45 \pm 0.13$	$1.1 \pm 0.06$
$36.69 \pm 0.13$	$1.1 \pm 0.06$
$36.17 \pm 0.12$	$1.1 \pm 0.06$
$35.54 \pm 0.12$	$1.1 \pm 0.06$
$34.58 \pm 0.12$	$1.1 \pm 0.06$
$33.69 \pm 0.11$	$1.0 \pm 0.06$
$33.33 \pm 0.11$	$1.1 \pm 0.06$
$32.80 \pm 0.11$	$1.1 \pm 0.06$
$32.25 \pm 0.11$	$1.1 \pm 0.06$
$31.90 \pm 0.11$	$1.1 \pm 0.06$
$31.14 \pm 0.10$	$1.1 \pm 0.06$
$29.73 \pm 0.10$	$1.1 \pm 0.06$
$27.77 \pm 0.10$	$1.1 \pm 0.06$
$25.77 \pm 0.09$	$1.1 \pm 0.06$
$24.63 \pm 0.08$	$1.1 \pm 0.06$
$24.77 \pm 0.08$	$1.1 \pm 0.06$
$24.52 \pm 0.08$	$1.1 \pm 0.06$

## 5.6 Single Photon Calibration

With the integrated pulse height (IPH) we don't know how much photoelectrons (pe) are measured. We need to do a calibration. A blue LED in the setup and a pulse generator were used to produce a light signal of 10 ns width and a periodicity of 10.0  $\mu$ s. The LED was high with  $V_{high} = 1.7$  V and it was low with  $V_{low} = 1.0$  V.

The pulse generator was connected to the oscilloscope to trigger on the light pulse. Now we were able to measure single photon events and calculate the correction factor to extract the number of photoelectrons from the IPH. The number of photoelectrons divided by the number of photoelectrons at ideal purity is the light yield.

## 5.7 Quartz Plate Series in Gaseous Argon

The light of the slow decay component  $\tau_2$  should be emitted in the 128 nm band. We installed a quartz plate in front of the lower (Ch2) PMT to proof whether the light of the slow component is effectively from the 128nm VUV photons. Quartz has the property to filter all wavelengths below approximately 160 nm. We could observe an almost vanishing slow component  $\tau_2$  signal and a remaining peak of the fast component  $\tau_1$  on the lower PMT. That is because the photons of the fast decay component are emitted in gaseous argon above 150nm. The upper PMT was to show that the actual condition was in a steady state.

This measurement result gives strong evidence that the observed slow decay component  $\tau_2$  is from the 128 nm light band.

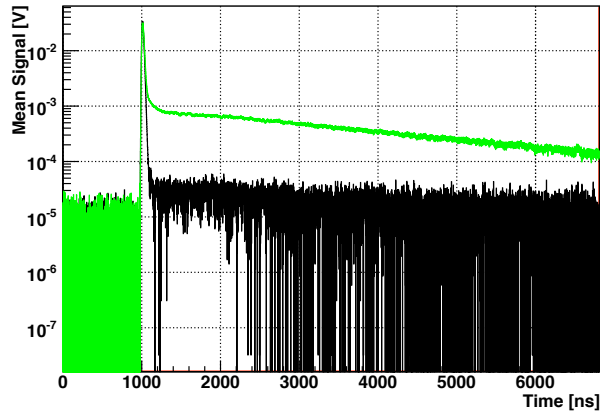


Figure 34: Average pulse shape of gaseous argon measurement with a quartz ( $SiO_2$ ) plate on the lower photomultiplier (black trace). The top curve (green) is from the PMT without quartz absorption. The presented data (first series) are acquired shortly after filling the vessel with argon. The signal is cut off below a pulse height of 0.014 V and above 0.2 V.

## 6 Summary

The time dependence of luminescence for liquid argon was measured under different conditions using an argon cell with sidewall reflectors. The reflectors are made with four different TPB surface densities. In four measurement sets we tested the effect of the TPB concentration under LAr conditions. The purpose was to measure the light yield for each reflector. During the work an effect of decreasing light yield with time was observed that is not understood yet.

Further measurements were done under gaseous argon conditions: decrease of the slow decay component  $\tau_2$  with time; proof of the 128 nm band as the origin of the slow decay component  $\tau_2$ .

## 7 Final Results and Conclusion

In the analyzed data we can observe a decreasing light yield with time for all four reflectors as shown in the figures 39, 37, 38, and 36. We see that the maximum light yield on the very beginning of the measurement is unstable. Due to this effect it is not reasonable to compare the maximum light yield of the four different reflectors with each other. The light yield approaches an asymptotic value, that is the minimum as we can see in fig. 39, 37, 38, and 36 (The four plots are done with a different data analysis [executed by V. Boccone] than fig. 35 and are only to clarify the decreasing light yield).

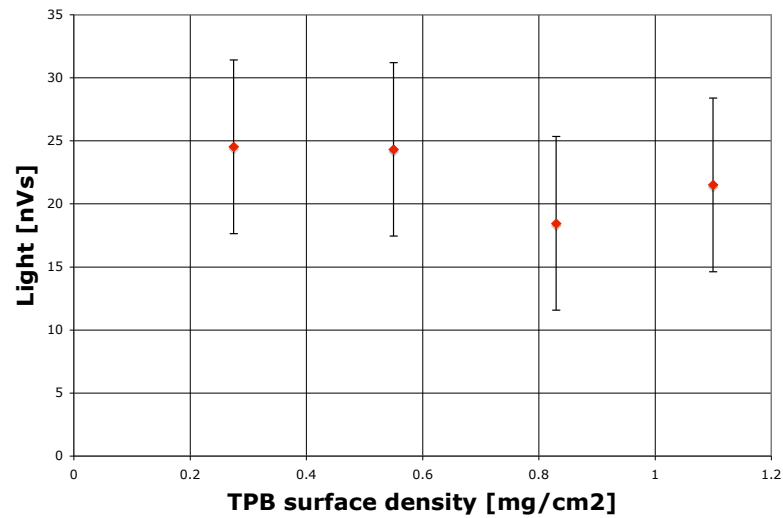


Figure 35: The plot shows the minimal value of the integrated pulse height for each reflector vs. TPB surface density on the reflector. The values are from the measured series on the table 1, 2, 3 and 4.

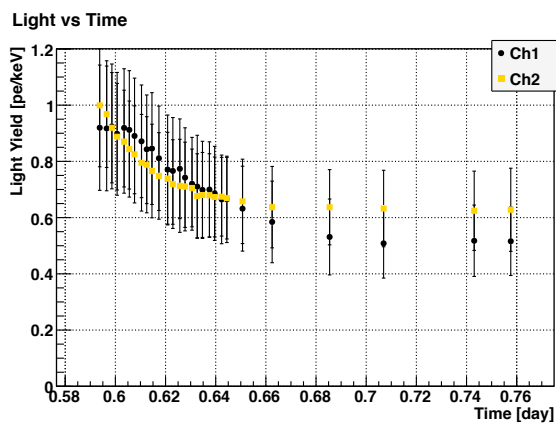


Figure 36: Light yield vs. time for the reflector with 1.10 mg/cm<sup>2</sup> TPB surface density

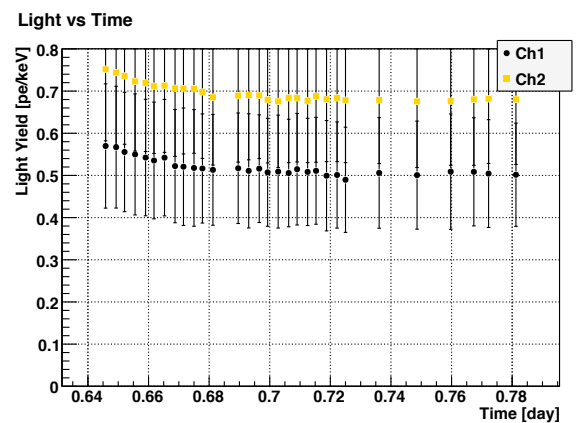


Figure 37: Light yield vs. time for the reflector with 0.55 mg/cm<sup>2</sup> TPB surface density

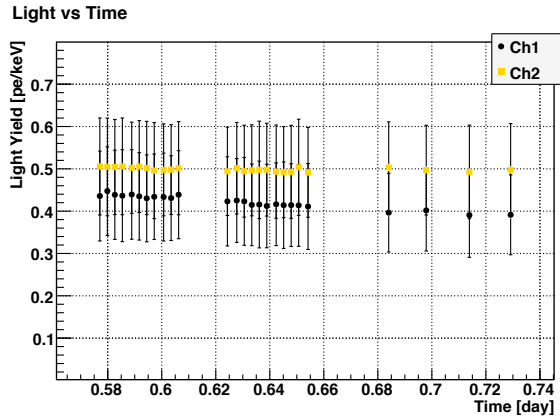


Figure 38: Light yield vs. time for the reflector with  $0.25 \text{ mg/cm}^2$  TPB surface density

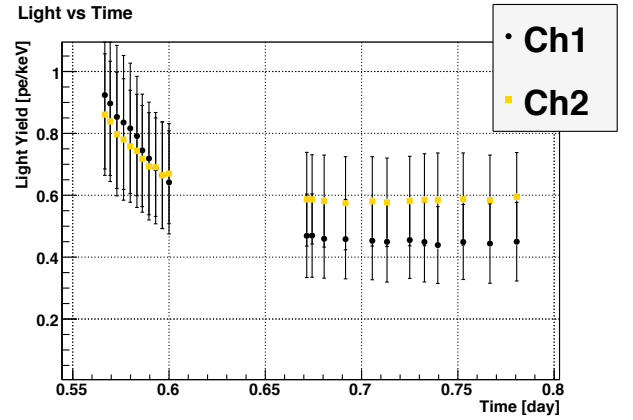


Figure 39: Light yield vs. time for the reflector with  $0.80 \text{ mg/cm}^2$  TPB surface density

The minimal values of the integrated pulse height for the four different reflector types are in a very close range (fig. 35). The conclusion is that we have no significant change of the light yield for different TPB surface densities in the range I test the reflectors ( $0.25$ ,  $0.55$ ,  $0.80$  and  $1.1 \text{ mg/cm}^2$  TPB). This result is sustained by the published conclusions of R. Chandrasekharan[12]. At the present time ArDM is using  $1.0 \text{ mg/cm}^2$  TPB. That means the surface density can be lowered to  $0.25 \text{ mg/cm}^2$  TPB without losing light yield.

The effect that absorbs the IPH with time was measured the first time in this experimental setup in such a strong way. The reason for this IPH shift behaviour is unclear. It might be that the gain of the PMTs decreases due to changing temperature. But the conditions (liquefaction speed, start time of the data acquisition, internal electronics, high voltage etc.) were the same for all four measurements. But the absorption effect is different in each measurement. So we probably can exclude this reason.

Further investigations with high gain PMTs have to be done to confirm this effect and to exclude possible sources on the measurement hardware that could cause this behaviour of a decreasing light yield.

Since the goal is to achieve steady and well understood conditions for future WIMP-event detection there are other effects that have much greater influence on the measurements than the TPB surface density on the reflector. Effects caused by impurities in the LAr such as absorption of scintillation light or change of the decay time of the excited argon molecules will play a major role in the light readout system.

## 8 Acknowledgements

I thank Prof. Claude Amsler who gave me the opportunity to realize this work for my bachelor thesis in his group at CERN.

I thank Vittorio Boccone for his effort, the great support and the most useful advices! Dr. Christian Regenfus I would like to thank for numerous excellent talks and instructive advices.

It was a good time in the particle physics group of the University of Zurich at CERN. I benefited a lot for my understanding in physics and gained major knowledge in research of particle physics.

I highly recommend this opportunity to all physics students and hope many will do this experience at CERN.

## References

- [1] C. Amsler, *Kern- und Teilchenphysik*, vdf Hochschulverlag AG / UTB Uni-Taschenbücher GmbH
- [2] H. Cabrera, *Optimierung des Wellenlängenschiebers für das ArDM-Experiment*, Master thesis, University of Zurich, 2007
- [3] C. Amsler et al., *Luminescence quenching of the triplet excimer state by air traces in gaseous argon*, Journal of Instrumentation 3 (2008) P02001
- [4] C. Amsler et al., *Towards a dark matter experiment*, Jahresbericht 2006, Physikinstitut, University of Zurich
- [5] *3M Vikuiti film specifications*, [http://solutions.3m.com/wps/portal/3M/en\\_US/Vikuiti1/BrandProducts/secondary/customersupport/faq/](http://solutions.3m.com/wps/portal/3M/en_US/Vikuiti1/BrandProducts/secondary/customersupport/faq/) , January 2008
- [6] A. Büchler, *The beginning of a dark matter adventure*, Bachelor thesis 2006
- [7] P. Cennini et al., *Detection of scintillation light in coincidence with ionizing tracks in a liquid argon time projection chamber*, Nuclear Instruments and Methods in Physics Research, A 432 (1999) 240
- [8] C. Regenfus, *Detection of VUV scintillation light in one ton of liquid argon*, Physik-Institut, University of Zurich (2007)
- [9] R. Chandrasekharan, M. Messina, A. Rubbia *Detection of noble gas scintillation light with large area avalanche photodiodes (LAAPDs)*, Nuclear Instruments and Methods in Physics Research A 546 (2005) 426
- [10] L. Kaufmann and A. Rubbia, *The ArDM project: a Dark Matter Direct Detection Experiment based on Liquid Argon*, Institute for Particle Physics, ETH Zurich

- [11] Hitachi et al., *Effect of ionization density on the time dependence of luminescence from liquid argon and xenon*, Phys. Rev. B, 1983
- [12] R. Chandrasekharan *Design of the light readout for the ArDM experiment*, Dissertation, ETH Zürich 2007

## 9 Glossary

ESR - Enhanced Specular Reflector

IPH - Integrated Pulse Height

LAr - liquid argon

LEM - Large Electron Multiplier

PMT - photomultiplier tube

TPB - wavelength shifting substance Tetra Phenyl Butadiene

PTFE - Polytetrafluoroethylene is a synthetic fluoropolymer that finds numerous applications and is well known under his brand name Teflon.

VUV light - vacuum ultra-violet em radiation in the range of 50 - 180 nm

SUSY - Super Symmetric System

TTX - Tetratex membrane (white Tetratex PTFE membrane), which provides permeability to gases, chemical inertness, diffusion of UV-photons and softness at cryogenic temperature PMT

WIMP - Weak Interacting Massive Particle

WLS - wavelength shifter

3M - technology company